Korean J. Chem. Eng., 35(8), 1620-1625 (2018)
DOI: 10.1007/s11814-018-0071-3

pISSN: 0256-1115
eISSN: 1975-7220

Anion-exchange-membrane-based electrochemical synthesis of ammonia as a carrier of hydrogen energy

Jong Hyun Park*,, Hyung Chul Yoon*, Jong-Nam Kim*, Chan-Hee Jeong*, Eun-Young Jeong*, Dae Sik Yun*, Hana Yoon*, Sang Hyun Park*, Moon-Hee Han**,†, and Chung-Yul Yoo*,†**

*Korea Institute of Energy Research, 152 Gajeong-ro, Yuseong-gu, Daejeon 34129, Korea
**Graduate School of Energy Science and Technology, Chungnam National University, 99 Daehak-ro, Yuseong-gu, Daejeon 34134, Korea
(*Received 21 January 2018 • accepted 30 April 2018*)

Abstract−With a 17.6 wt% hydrogen content, ammonia is a non-carbon-emitting, easy to store and transport, carrier of hydrogen energy. In this study, an anion-exchange-membrane-based (AEM-based) electrochemical cell was used to electrochemically synthesize ammonia from water and nitrogen under ambient conditions. The electrochemical cell was fabricated by attaching Pt/C to both sides of the AEM, and ammonia was generated by supplying nitrogen gas to the cathodic chamber of the cell. AC impedance and current-voltage (I-V) properties were analyzed in relation to the externally applied voltage, and ammonia-formation rates and faradaic efficiencies were determined. The maximum ammonia-formation rate was 1.96×10^{-11} mol·s^{-1}·cm^{-2} at an applied voltage of 2 V, with a faradaic efficiency of 0.18%.

Keywords: Anion-exchange Membrane, Alkaline Water Electrolysis, Electrochemical Ammonia Synthesis

INTRODUCTION

Environmental change resulting from climate change has recently stimulated considerable research activity into renewable energy that is not associated with greenhouse gas emissions. However, since renewable energy is unevenly distributed spatially and is temporally intermittent, energy-storage technology is required to overcome these drawbacks. Secondary batteries, which are typical energy storage devices, have limited storage capacities; consequently, research into the conversion, storage, and use of renewable energy in the form of transportable chemical energy is required to overcome these issues. Power-to-gas (P2G) technology, in which renewable electrical energy is converted into a gaseous fuel, is the most widely studied conversion technology [1], with hydrogen, which can be synthesized by the electrolysis of water, the most widely studied gaseous fuel. However, as an energy carrier, hydrogen is difficult to store and transport. To overcome these drawbacks, ammonia is attracting growing interest as an energy carrier since it is easier to store and transport, and only emits water and nitrogen through complete combustion [2].

Ammonia is a hydrogen reservoir (17.6 wt% H_2), has 100-to-1,000 times the weight percentage of gaseous or liquid hydrogen, and has an energy density per weight or volume similar to that of fossil fuel (e.g., coal and oil) [3]. Furthermore, once NH_3 is liquefied (pressure of 7.5 at 25 °C), ammonia is considerably safer than ethanol, gasoline, and diesel from the perspectives of vapor pressure, IDLH (immediately dangerous to life or health) value, relative toxicity, flash point, and explosion limit [4]. To date, ammonia has been commercially synthesized using the Haber-Bosch process, in which ammonia is produced by reacting nitrogen, separated from air, with hydrogen, obtained through fossil-fuel reforming, at high temperatures (450 to 500 °C) and high pressures (150 to 300 bar) [5]. However, the Haber-Bosch process is energy intensive and emits large amounts of CO_2, which is problematic [6]. Therefore, the production of ammonia using renewable energy in a non-Haber-Bosch process not only overcomes the limitations of temporal discontinuity and uneven spatial distribution, but also avoids CO_2 emissions. Not only is ammonia easier to store and transport than hydrogen, it has other applications in areas such as hydrogen-based fuel, fertilizers, fuel cells, internal combustion engines, and explosives [7-9].

To overcome problems associated with the Haber-Bosch process, studies into the synthesis of ammonia through the electrochemical reaction of hydrogen (or water vapor) with nitrogen, at a lower temperature and pressure than those used in the Haber-Bosch process, have been conducted [7,10-13]. In 1998, Marnellos et al. [14] reported the electrochemical synthesis of ammonia using a solid proton (H^+) electrolyte. Since then, several studies into ammonia-synthesis methods using solid-state electrolytes have been reported, including an electrochemical method using water vapor and nitrogen. Furthermore, studies into the synthesis of ammonia using various types of solid electrolyte that are proton- or oxide-conducting (O^{2-}-conducting) molten-salt electrolytes have been reported [11,15-19], as well as processes that use electrocatalysts that promote nitrogen dissociation. Solid polymer electrolytes (SPEs) can overcome the disadvantages of solid-state ammonia synthesis, such as ammonia decomposition at high temperatures, and high cost. Studies into the electrochemical synthesis of ammonia using SPEs have mainly focused on Nafion membranes [20-27] or anion-exchange membranes (AEMs) [28]. More recently, Renner et al. [28] reported the synthesis of ammonia using Pt, Fe, Ni, or FeNi

†To whom correspondence should be addressed.
E-mail: cyoo@kier.re.kr, mhhan@cnu.ac.kr

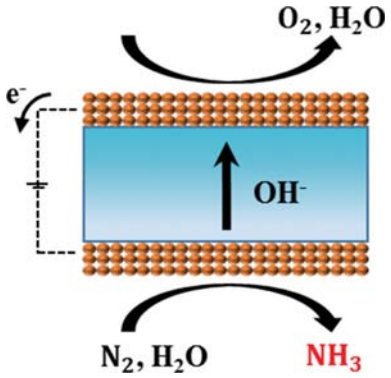

Fig. 1. Depicting the electrochemical synthesis of ammonia from water and nitrogen using a conducting hydroxide (OH^-) electrolyte.

as the electrocatalyst and an AEM instead of the conventionally used Nafion electrolyte membrane; the ammonia formation rate was reported to be (1.33-3.80)×10^{-12} mol·cm^{-2}·s^{-1} at 50 °C and 1.2 V, with a faradaic efficiency of 1.1-41%. In addition, the energy consumption of the AEM-based electrochemical process (14 kWh/kg_{NH3}) is comparable to that of the Haber-Bosch process (13.2 kWh/kg_{NH3}). The AEM is a hydroxide-conductive (OH^--conductive) electrolyte membrane with a similar ionic conductivity to that of Nafion. In this study, we chose to use an anion-exchange membrane over an acidic membrane (e.g. Nafion) because NH_3 is a weak base that can react with an acidic membrane, resulting in the deterioration of its ionic conductivity in an NH_3-containing atmosphere, as reported in the literature [29,30]. Furthermore, direct ammonia fuel cells using anion-exchange membranes have been successfully demonstrated [31,32], confirming the stable nature of anion-exchange membranes in NH_3-containing atmospheres.

Fig. 1 displays the overall process for the electrochemical synthesis of ammonia from water and nitrogen using a hydroxide-conductive electrolyte, with the detailed chemical steps shown in Eq. (1). At the reducing electrocatalyst/electrolyte interface, water and nitrogen are simultaneously dissociated to form ammonia. Hence, the cathodic electrocatalyst should not only dissociate nitrogen, but also perform effective water electrolysis to supply protons for electrochemical ammonia synthesis.

$$\begin{aligned}&\text{anode: } 12OH^- \rightarrow 3O_2+6H_2O+12e^- \qquad E_a^0=0.401\text{ V (vs. SHE)}\\&\text{cathode: } 2N_2+12H_2O+12e^- \rightarrow 4NH_3+12OH^-\\&\qquad\qquad E_c^0=-0.771\text{ V (vs. SHE)} \quad (1)\\&\text{overall reaction: } 2N_2+12H_2O \rightarrow 4NH_3+3O_2+6H_2O\\&\qquad\qquad E_{total}^0=1.171\text{ V (vs. SHE)}\end{aligned}$$

While numerous previous studies into the electrochemical synthesis of ammonia using Nafion SPE membranes have been reported, to the best of our knowledge only few studies used an AEM [28,33-35], and no studies that investigate the electrochemical characteristics and effect of applied voltage, have appeared. We now report a systematic analysis of the electrochemical characteristics of AEM-based electrochemical cells and their performance during the synthesis of ammonia from water and nitrogen.

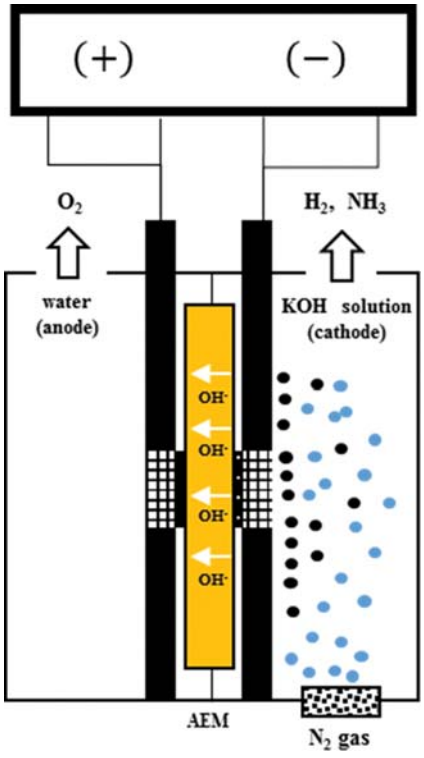

Fig. 2. The electrochemical cell used for the synthesis of ammonia.

EXPERIMENTAL

The system used for the electrochemical synthesis of ammonia is shown in Fig. 2. A commercial AEM (FAAM-40, quaternized polysulfone membrane in bromide form) was purchased from Fumatech. The anode and cathode were both 20% Pt-on-carbon-cloth electrodes (Fuel Cell Earth, EC2019, 0.5 mg/cm^2). To prepare the membrane-electrode assembly, the Pt-on-carbon-cloth electrodes were attached symmetrically to both sides of the AEM by mechanical pressing. Prior to the electrochemical ammonia synthesis, the membrane-electrode assembly was immersed in 6 M KOH solution to exchange hydroxide for bromide in the AEM [36]. A 30 wt% KOH solution was prepared by dissolving potassium hydroxide (Junsei, Guaranteed reagent, ASSAY(KOH) min. 85.0% (w/w)) in deionized water (18.2 MΩ·cm). Titanium gauze (80 mesh, 3×3 cm) was used as the current collector in the electrochemical cell, and the remaining components were coated with Teflon. Nitrogen (99.999%) was continuously bubbled into the cathodic chamber at a flow rate of 100 mL/min. The microstructure of Pt-on-carbon-cloth electrode was characterized by means of scanning electron microscope (SEM, Hitachi S-4700). Electrochemical analyses were performed using an electrochemical impedance analyzer (Metrohm, Autolab PGSTAT302N) and electrochemical impedance spectroscopy (EIS) was performed over the 1 MHz to 0.01 Hz frequency range. The concentrations of captured ammonia and hydrazine were analyzed quantitatively using a UV-vis spectrophotometer (Shimadzu UV 1600) and a 10×10 mm JM-CQ001 quartz cell (JM Science). Gaseous ammonia was captured using sulfuric acid (0.1 N, OCI Company Ltd.). Ammonia produced at the cath-

ode of the electrochemical cell was captured with 30 mL of 0.001 M aqueous sulfuric acid. These procedures were repeated three times at each applied voltage, and the means and standard errors in the formation rates of ammonia (NH_3) and hydrazine (N_2H_4) were calculated.

The captured ammonia gas was analyzed using the indophenol method, in which the concentration of ammonia is determined by measuring the absorbance of indophenol blue produced through the reaction of indophenol and ammonium ions (NH_4^+) in the presence of hypochlorite. The NH_3-formation rate and the corresponding faradaic efficiency were calculated using Eqs. (2) and (3):

$$r_{NH_3}\,(\mathrm{mol\cdot cm^{-2}\cdot s^{-1}}) = \frac{x(\mathrm{mg/L})\times 10^{-3}(\mathrm{g/mg})\times V(\mathrm{L})}{Mr_{NH_4}(\mathrm{g/mol})\times t(\mathrm{s})\times A(\mathrm{cm^2})} \quad (2)$$

$$FE_{NH_3}\,(\%) = \frac{3\times F\times r_{NH_3}\times t(\mathrm{s})\times A(\mathrm{cm^2})}{Q(\mathrm{C})}\times 100\% \quad (3)$$

where x(mg/L) refers to the concentration of the generated ammonium ions [NH_4^+], V(L) refers to the total volume of the diluted sulfuric acid solution (0.001 M) used to capture ammonia, $Mr_{NH_4^+}$ is the molecular weight of NH_4^+, t(s) is the ammonia-gas capture time, and A(cm^2) refers to the area of the electrode in the electrochemical cell.

It has been reported that hydrazine (N_2H_4) can be formed as a by-product together with NH_3 through the nitrogen reduction reaction via an associative mechanism [17]. The rate of N_2H_4 formation and the corresponding faradaic efficiency were calculated using Eqs. (4) and (5):

$$r_{N_2H_4}\,(\mathrm{mol\cdot cm^{-2}\cdot s^{-1}}) = \frac{x(\mathrm{mg/L})\times 10^{-3}(\mathrm{g/mg})\times V(\mathrm{L})}{Mr_{N_2H_4}(\mathrm{g/mol})\times t(\mathrm{s})\times A(\mathrm{cm^2})} \quad (4)$$

$$FE_{N_2H_4}\,(\%) = \frac{4\times F\times r_{N_2H_4}\times t(\mathrm{s})\times A(\mathrm{cm^2})}{Q(\mathrm{C})}\times 100\% \quad (5)$$

where the symbols in Eq. (4) have the same meanings as described in Eq. (2). In Eqs. (3) and (5), F is the Faraday constant (96,485 C/mol), r_{NH_3} and $r_{N_2H_4}$ refer to the ammonia- and hydrazine-formation rates, respectively, and t(s) refers to the ammonia and hydrazine capture times, Q(C) is the amount of charge induced by the applied voltage, and A(cm^2) refers to the area of the electrode in the electrochemical cell. The amount of hydrazine was analyzed using the p-dimethylaminobenzaldehyde (p-DAB) method. The concentration of hydrazine determined by measuring the absorbance of p-DAB. The formed product undergoes condensation reaction to form the hydrazone with p-DAB. The formed intensely yellow colored hydrazone. Hydrazine levels are determined by comparison with standard calibration curve. Figs. 3(a) and (b) display cali-

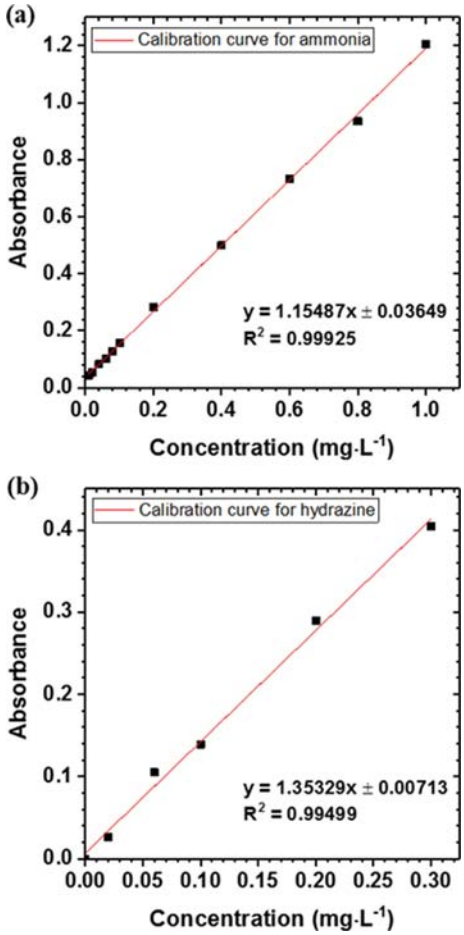

Fig. 3. (a) Calibration curve for ammonia. (b) Calibration curve for hydrazine.

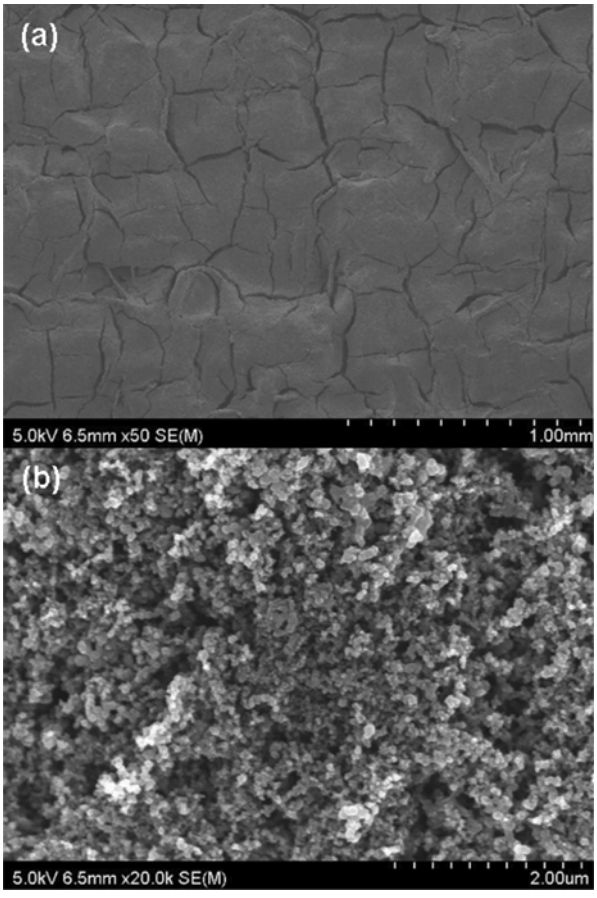

Fig. 4. SEM image of Pt-on-carbon-cloth electrode under low magnification (x50, (a)) and high magnification (x20k, (b)).

bration curves used for quantitative analyses; these curves were constructed using ammonia and hydrazine standards. The ammonia and hydrazine concentrations were determined by comparing the absorbances of blank and capture solutions at the maximum absorbance wavelengths of ammonia and hydrazine (635 nm and 456 nm, respectively) [37-41].

RESULTS AND DISCUSSION

Fig. 4 shows the microstructure of Pt-on-carbon-cloth electrode. The used Pt-on-carbon-cloth electrode exhibits typical gas diffusion electrode structure showing cracks at the surface under low magnification SEM (×50, Fig. 4(a)), while sub-micron spherical particles are observed under high magnification SEM (x20k, Fig. 4(b)). This structure could facilitate both N_2 gas diffusion and water electrolysis reaction to supply proton for the electrochemical ammonia synthesis at the surface of the Pt-on-carbon-cloth electrode facing the KOH solution.

Fig. 5(a) displays EIS spectra (Nyquist plots) at different applied voltages in the electrochemical cell at room temperature, from the open-circuit voltage (OCV) to 2.5 V; the upper-right inset shows

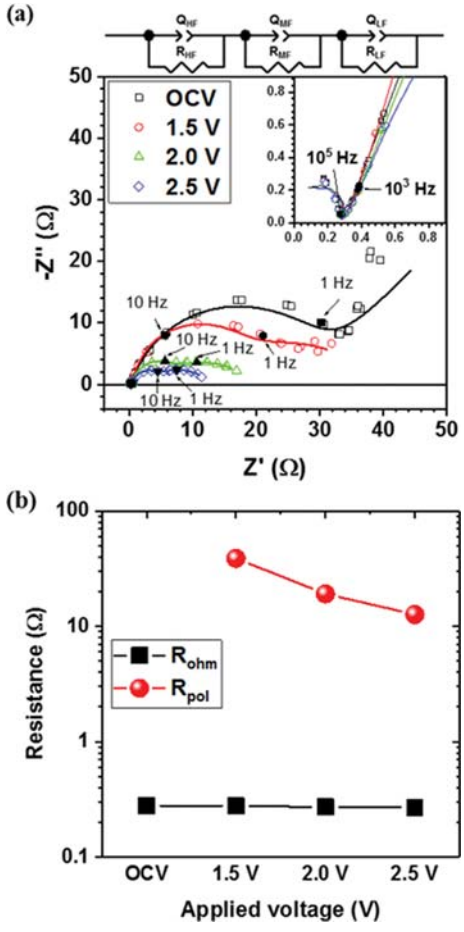

Fig. 5. (a) AC-impedance spectra in the 1.5-2.5 V applied voltage range. (b) Electrolyte (R_{ohm}) and polarization (R_{pol}) resistances of the electrochemical cell obtained from impedance spectroscopy. Frequencies are indicated on each spectrum.

an enlargement of the high-frequency region. The equivalent circuit is also displayed. The ZView impedance-analysis software (Scribner Associates, Inc.) was used for data analysis. The EIS data for the electrochemical cell can be described using an equivalent circuit composed of three resistors, each represented by constant-phase elements, using (R_{HF}, Q_{HF})(R_{MF}, Q_{MF})(R_{LF}, Q_{LF}), where R_{HF} and Q_{HF} refer to the resistance components of the electrolyte, R_{MF} and R_{LF} refer to the resistance components (R_{MF}, R_{LF}), and constant phase elements (Q_{MF}, Q_{LF}) in the mid-frequency (MF) and low-frequency (LF) regions of the electrode polarization process [42]. The impedance spectra reveal that the small semicircles in the mid-frequency region and the large semicircles in the low-frequency region appear to merge with increasing applied voltage. Typically, mid-frequency semicircles correspond to contributions from charge transfer-reaction, while low-frequency semicircles correspond to mass-transfer reactions [43].

The enlargement in Fig. 5(a) reveals that although different voltages were applied, the electrolyte resistances did not change in the high-frequency range, which confirms that the electrical conductivity of the electrolyte did not change. As shown in Fig. 5(b), under OCV conditions, the electrolyte resistance resulting from the applied voltage is 0.282 Ω and the corresponding electrical conductivity is 0.32 mS·cm^{-1}. Under OCV conditions, the impedance semicircle (the large central semicircle) in the mid-frequency region is much larger when voltage is applied. A large impedance semicircle (R_{MF}) indicates that diffusion is limited due to increases in charge-transfer resistance. The EIS spectrum under OCV condition reveals that the vertical line increasing in the direction from the semicircle to the imaginary component shows that mass-transfer resistance is greatly presented. Fig. 5(b) reveals that the polarization resistance (R_{MF}+R_{LF}) decreases to 31.9 Ω at an applied voltage of 1.5 V, with further decreases to 11.4 and 5.7 Ω at 2.0 and 2.5 V, respectively. Increasing the applied voltage stimulates the electrochemical reaction resulting in a decrease in charge-transfer and mass transfer resistances.

Fig. 6(a) displays the current density across the electrochemical cell as a function of time during the ammonia-synthesis experiment under different voltage conditions (1.5-2.5 V), at room temperature for 10 min, which reveals stable current densities in the applied voltage range. Furthermore, the current density increased as the applied voltage was increased in 0.5 V intervals, from 1.5 V to 2.5 V, resulting in the transfer of additional OH^- from the cathode to the anode. Although the initial current density was 0.83 mA·cm^{-2} at an applied voltage of 1.5 V, the current density gradually decreased to 0.21 mA·cm^{-2} over time. The initial current density was 2.65 mA·cm^{-2} at 2.0 V, which decreased to 2.5 mA·cm^{-2} after 600 s, while the initial current density was 6.98 mA·cm^{-2} at 2.5 V, and was 6.06 mA·cm^{-2} after 600 s. The large decrease in current density at 1.5 V is ascribable to current loss resulting from activation of the electrochemical cell at the start of the experiment, while current losses at 2.0 and 2.5 V were small because the electrochemical cell had already been activated. The current densities at 2.0 and 2.5 V were, respectively, 11-fold and 29-fold higher than that at 1.5 V.

Fig. 6(b) shows the ammonia formation rate and faradaic efficiency as functions of applied voltage calculated using the ammonia concentrations from the ammonia-synthesis experiment as well

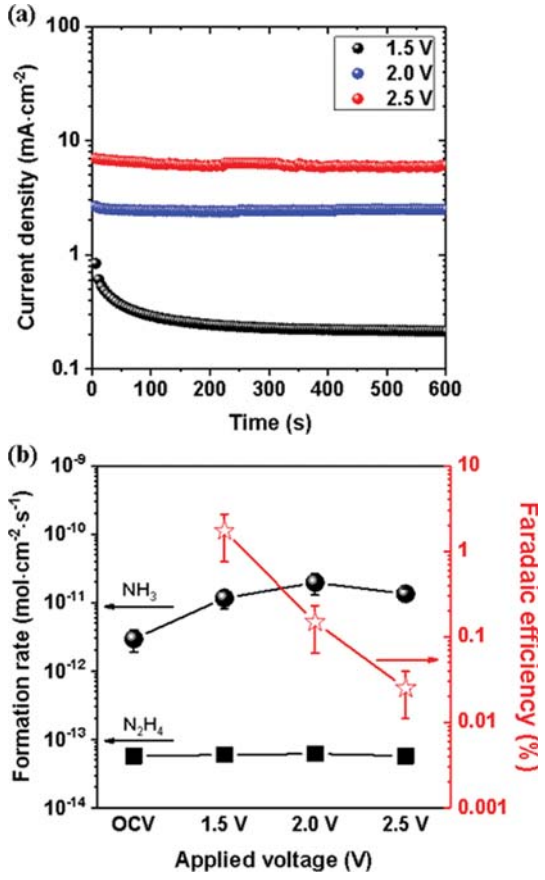

Fig. 6. (a) Current densities as functions of time over the 1.5-2.5 V applied voltage range. (b) Ammonia and hydrazine formation rates and faradaic efficiencies as functions of applied voltage. Error bars represent 95% confidence intervals around the means; when not shown, these errors are smaller than the size of the symbol.

as the current densities in Fig. 6(a). The ammonia formation rate was found to be 2.95×10^{-13} mol·cm^{-2}·s^{-1} under OCV conditions, which is similar to results reported in the literature for conventional solid-state ammonia syntheses; an ammonia formation rate of 8.8×10^{-12} mol·cm^{-2}·s^{-1} was reported under OCV conditions at 500 °C in the absence of an applied voltage when $BaZr_{0.8}Y_{0.2}O_{3-\delta}$ was used as a proton-conducting electrolyte and Ag was used as the electrocatalyst [15]. We postulate three reasons for the trace levels of ammonia produced in our experiment, despite OCV conditions. (i) The current applied to the electrochemical cell is low, as determined from impedance measurements prior to the experiment; (ii) trace amount of ammonia might be produced by the catalytic reaction of water and nitrogen were observed on the Pt/C cathode surface [44]; and (iii) the polyaromatic chemical structure of the AEM, which bears amino groups, only produces trace amounts of ammonia through the reactions of the tertiary amine groups with the KOH solution [45].

As shown in Fig. 6(b), the maximum ammonia formation rate was 1.96×10^{-11} mol·cm^{-2}·s^{-1} at an applied voltage of 2 V, and the overall faradaic efficiency was 0.148%. In previous studies on the AEM-based synthesis of ammonia [28,33-35], the maximum ammonia formation rate and faradaic efficiency were reported to be 4.05×10^{-11} mol·cm^{-2}·s^{-1} and 0.01%, respectively, which means that the faradaic efficiency in our experiment is 18-times higher than the highest value previously reported, despite similar ammonia-formation rates. These results may be attributable to the asymmetric structure of the cathode, which can facilitate both N_2-gas diffusion and proton supply. AEM-based electrochemical ammonia synthesis data are summarized in Table 1, which reveals that the AEM-based electrochemical-synthesis method in this study has a comparatively high ammonia formation rate and a much higher faradaic efficiency than the values in the literature. In the present experiment, the ammonia formation rate initially increased as the voltage was increased from 1.5 to 2 V before decreasing again, since, with increasing voltage, the hydrogen-evolution reaction is promoted at the expense of ammonia formation at the cathode, thereby limiting the synthesis of ammonia [25]. The hydrazine formation rate was $(5.77\text{-}6.19)\times10^{-14}$ mol·cm^{-2}·s^{-1} under different applied voltage conditions, which indicates a trace amount of hydrazine formation when compared to ammonia production, and no significant increase in hydrazine formation was observed as the applied voltage was increased from 1.5 to 2.5 V. The maximum overall faradaic efficiency (1.73%) for ammonia formation, observed at an applied voltage of 1.5 V, tended to decrease with increasing voltage. The observed decrease in faradaic efficiency with increasing applied voltage is ascribed to the preferential formation hydrogen gas over nitrogen reduction facilitated by the increase in current across the electrochemical cell when high voltages are applied at the cathode [46]. Additional investigations that explore novel electrocatalysts and processes that further promote the nitrogen-reduction reaction rather than the hydrogen-evolution reaction are required.

CONCLUSIONS

We showed that an AEM can also be used for the electrochem-

Table 1. Survey of AEM-based electrochemical ammonia synthesis results

	Anode	Cathode	Maximum NH_3 formation rate (mol·cm^{-2}·s^{-1})	Faradaic efficiency (%)	Reference
1	Not specified-	Pt, Fe, Ni, FeNi	3.80×10^{-12}	1.1-41	[28]
2	Pt/C	Pt, Ir, Pd, Ru, Au	2.09×10^{-12}	0.55	[33]
3	Pt/C(IrO_2)	Pt/C(γ-Fe_2O_3)	3.72×10^{-14}	0.011	[34]
4	Pt/C	Pt/C	4.05×10^{-11}	0.01	[35]
5	Pt/C	Pt/C	1.96×10^{-11}	0.18	This study

ical synthesis of ammonia from water and nitrogen. Electrochemical impedance spectroscopy revealed that the Pt/C-AEM-Pt/C electrolyte resistance remained constant in the 1.5 to 2.5 V applied-voltage range. We showed that the impedance semicircle in the Nyquist plot, which represents a combination of charge-transfer and mass-transfer resistances, decreased with increasing applied voltage. The maximum rate of ammonia formation was determined to be 1.96×10^{-11} mol·cm^{-2}·s^{-1} at an applied voltage of 2 V; compared with previous studies using AEMs, this value represents an 18-fold increase in the faradaic efficiency. When a voltage in excess of 2 V was applied to the electrochemical cell, the hydrogen evolution reaction was promoted at the cathode at the expense of ammonia production, resulting in a decrease in the rate of ammonia formation. The maximum faradaic efficiency was 1.73% at 1.5 V.

ACKNOWLEDGEMENTS

This work was conducted under the framework of the Research and Development Program of the Korea Institute of Energy Research (KIER) (B8-2434).

REFERENCES

1. M. Götz, J. Lefebvre, F. Mörs, A. McDaniel Koch, F. Graf, S. Bajohr, R. Reimert and T. Kolb, *Renew. Energy*, **85**, 1371 (2016).
2. A. Klerke, C. H. Christensen, J. K. Nørskov and T. Vegge, *J. Mater. Chem.*, **18**, 2304 (2008).
3. A. Züttel, A. Remhof, A. Borgschulte and O. Friedrichs, *Philos. Trans. A Math. Phys. Eng. Sci.*, **368**, 3329 (2010).
4. T. Zhang, H. Miyaoka, H. Miyaoka, T. Ichikawa and Y. Kojima, *ACS Appl. Energy Mater.*, **1**, 232 (2018).
5. M. Boudart, *Top. Catal.*, **1**, 405 (1994).
6. M. Reese, C. Marquart, M. Malmali, K. Wagner, E. Buchanan, A. McCormick and E. L. Cussler, *Ind. Eng. Chem. Res.*, **55**, 3742 (2016).
7. R. Lan, J. T. S. Irvine and S. Tao, *Int. J. Hydrog. Energy*, **37**, 1482 (2012).
8. Y. Bicer and I. Dincer, *J. Clean. Prod.*, **170**, 1594 (2018).
9. S. Kim, J. Song and H. Lim, *Korean J. Chem. Eng.*, **35**, 1 (2018).
10. S. Giddey, S. P. S. Badwal and A. Kulkarni, *Int. J. Hydrog. Energy*, **38**, 14576 (2013).
11. I. A. Amar, R. Lan, C. T. G. Petit and S. Tao, *J. Solid State Electrochem.*, **15**, 1845 (2011).
12. V. Kyriakou, I. Garagounis, E. Vasileiou, A. Vourros and M. Stoukides, *Catal. Today*, **286**, 2 (2017).
13. A. R. Singh, B. A. Rohr, J. A. Schwalbe, M. Cargnello, K. Chan, T. F. Jaramillo, I. Chorkendorff and J. K. Nørskov, *ACS Catal.*, **7**, 706 (2017).
14. G. Marnellos and M. Stoukides, *Science*, **282**, 98 (1998).
15. D. S. Yun, J. H. Joo, J. H. Yu, H. C. Yoon, J.-N. Kim and C.-Y. Yoo, *J. Power Sources*, **284**, 245 (2015).
16. A. Skodra and M. Stoukides, *Solid State Ion.*, **180**, 1332 (2009).
17. C.-Y. Yoo, J. H. Park, K. Kim, J.-I. Han, E.-Y. Jeong, C.-H. Jeong, H. C. Yoon and J.-N. Kim, *ACS Sustainable Chem. Eng.*, **5**, 7972 (2017).
18. H. Jeoung, J. N. Kim, C.-Y. Yoo, J. H. Joo, J. H. Yu, K. C. Song, M. Sharma and H. C. Yoon, *Korean Chem. Eng. Res.*, **52**, 58 (2014).
19. K. Kim, C.-Y. Yoo, J.-N. Kim, H. C. Yoon and J.-I. Han, *Korean J. Chem. Eng.*, **33**, 1777 (2016).
20. V. Kordali, G. Kyriacou and C. Lambrou, *Chem. Commun.*, **17**, 1673 (2000).
21. G. Xu, R. Liu and J. Wang, *Sci. China Chem.*, **52**, 1171 (2009).
22. R. Liu, *Chin. J. Chem.*, **28**, 139 (2010).
23. Z. Zhang, Z. Zhong and R. Liu, *J. Rare Earth.*, **28**, 556 (2010).
24. R. Lan, J. T. S. Irvine and S. Tao, *Sci. Rep.*, **3**, 1145 (2013).
25. R. Lan and S. Tao, *RSC Adv.*, **3**, 18016 (2013).
26. S. Chen, S. Perathoner, C. Ampelli, C. Mebrahtu, D. Su and G. Centi, *Angew. Chem. Int. Ed.*, **56**, 2699 (2017).
27. S. Chen, S. Perathoner, C. Ampelli, C. Mebrahtu, D. Su and G. Centi, *ACS Sustainable Chem. Eng.*, **5**, 7393 (2017).
28. J. N. Renner, L. F. Greenlee, K. E. Ayres and A. M. Herring, *Electrochem. Soc. Interface*, **24**, 51 (2015).
29. F. A. Uribe, S. Gottesfeld and T. A. Zawodzinski, *J. Electrochem. Soc.*, **149**, 293 (2002).
30. R. Halseid, P. J. S. Vie and R. Tunold, *J. Power Sources*, **154**, 343 (2006).
31. R. Lan and S. Tao, *Electrochem. Solid-State Lett.*, **13**, 83 (2010).
32. S. Suzuki, H. Muroyama, T. Matsui and K. Eguchi, *J. Power Sources*, **208**, 257 (2012).
33. J. Nash, X. Yang, J. Anibal, J. Wang, Y. Yan and B. Xu, *J. Electrochem. Soc.*, **164**, 1712 (2017).
34. J. Kong, A. Lim, C. Yoon, J. H. Jang, H. C. Ham, J. Han, S. Nam, D. Kim, Y.-E. Sung, J. Choi and H. S. Park, *ACS Sustainable Chem. Eng.*, **5**, 10986 (2017).
35. B. L. Sheets and G. G. Botte, *Chem. Commun.* (2018), DOI:10.1039/c8cc00657a.
36. G.-J. Hwang, S.-G. Lim, S.-Y. Bong, C.-H. Ryu and H.-S. Choi, *Korean J. Chem. Eng.*, **32**, 1896 (2015).
37. I. Ivancic, *Water Res.*, **18**, 1143 (1984).
38. A. Aminot, D. S. Kirkwood and R. Kérouel, *Marine Chem.*, **56**, 59 (1997).
39. E. P. Felix and A. A. Cardoso, *Instrument. Sci. Technol.*, **31**, 283 (2003).
40. N. T. Crosby, *Analyst*, **93**, 406 (1968).
41. A. Afkhami and A. R. Zarei, *Talanta*, **62**, 559 (2004).
42. C.-Y. Yoo, D. S. Yun, S.-Y. Park, J. Park, J. H. Joo, H. Park, M. Kwak and J H. Yu, *Electrocatal.*, **7**, 280 (2016).
43. N. V. Dale, M. D. Mann, H. Salehfar, A. M. Dhirde and T. Han, *J. Fuel Cell Sci. Technol.*, **7**, 31010 (2010).
44. S. Kishira, G. Qing, S. Suzu, R. Kikuchi, A. Takagaki and S. T. Oyama, *Int. J. Hydrog. Energy*, **42**, 26843 (2017).
45. I. Garcia-Herrero, M. Alvarez-Guerra and A. Irabien, *J. Chem. Technol. Biotechnol.*, **91**, 507 (2016).
46. A. Sclafani, V. Augugliaro and M. Schiavello, *J. Electrochem. Soc.*, **130**, 734 (1983).